Loading and Power Control for A High-Efficiency Class E PA Driven Megahertz WPT System

Minfan Fu, *Member, IEEE,* He Yin, *Student Member, IEEE,* Ming Liu, *Student Member, IEEE,* Chengbin Ma, *Member, IEEE*

***Abstract*—In this paper, the loading effect of a Class E power amplifier (PA) driven 6.78 megahertz (MHz) wireless power transfer (WPT) system is analyzed at both circuit and system levels. A buck converter is introduced and controlled to track an optimal equivalent load that maximizes the system efficiency under uncertainties in the relative position of coils and the final load. For power control, an additional degree of freedom is provided by adding an ultracapacitor bank. A control strategy is proposed to track the maximum efficiency and charge/discharge the ultracapacitor bank through the on/off control of the Class E PA. Thus high system efficiency can be maintained under various uncertainties and load power demands. Finally, the theoretical analysis and the control scheme are validated in experiments. The results show that the proposed Class E PA driven MHz WPT system can stably achieve a high efficiency under different coil distances and various constant/pulsed power profiles. The measured highest system efficiency can reach 72.1% at a load power level of 10 W.**

***Index Terms*—Megahertz wireless power transfer, Class E power amplifier, maximum efficiency tracking, load power demand, ultracapacitor**

I. Introduction

Wireless power transfer (WPT) using inductive resonance coupling has become increasingly popular in recent years. Now it is being applied to charge wearable devices, cellphones, household appliances and even electric vehicles [1], [2]. Currently WPT working at kilohertz (kHz) shows rapid improvement thanks to the new development in power electronics [3]–[8]. Meanwhile, it is attractive to further increase the resonance frequency such as to several megahertz (MHz) especially for a higher level of spatial freedom, namely a longer transfer distance and higher tolerance to coupling coil misalignment. A higher frequency also helps to build more compact and lighter WPT systems. At the same time limitations exist in the performance of power electronic devices, the usable frequency range under the regulation of ISM (industrial, scientific, and educational) band, etc. Therefore WPT systems working at MHz are now widely considered to be suitable for low-power applications.

Parallel with the development of kHz WPT, MHz WPT has also attracted wide interest. Many works can be found in analysis, design, optimization, and control of MHz WPT systems. Circuit-level design and optimization include compensation of coils, high efficiency power amplifiers (PAs) and rectifiers, tunable circuits, etc [9]–[15]. In terms of control, frequency tuning is popular [16]. However it may violate the bandwidth constraint of the ISM band, which is narrow at MHz [17]. Variable capacitors and inductors can be used to achieve dynamic impedance matching for coils [18]–[20] and tunable inverters [21], [22]. These systems are based on switching among multiple passive components or use complicated tuning circuits. Dc-dc converters were applied to improve the robustness of the system performance such as the efficiency [23], [24]. Besides, a phased array WPT system was recently proposed for efficient power transfer and control of power delivery and leakage field strength [25].

This paper develops a control scheme that maintains a high efficiency of a Class E PA driven MHz WPT system. The Class E PA is known to be a promising power source working at high switching frequencies thanks to its simple topology and soft-switching property, i.e., zero-voltage switching (ZVS) and zero-voltage-derivative switching (ZVDS) [26]–[28]. Meanwhile, in real applications difficulties in the control arise from various power demands and uncertainties such as variations in the relative position of coils and load characteristic. This problem becomes even more challenging for a WPT system driven by the Class E PA due to the high load sensitivity of the PA [26], [29], [30]. Furthermore, the impedance characteristics of circuits at MHz are much more complicated than those in the conventional kHz band studied in power electronics. This difference causes additional difficulty in achieving an optimized operation of a MHz WPT system. New configuration, comprehensive system-level analysis, and suitable control strategies are expected that provide a solution to maintain a high efficiency of the WPT system under various uncertainties and power demands.

To the knowledge of the authors, this paper represents one of the first attempts to provide system-level analysis and optimization (i.e., from source to final load) of a MHz WPT system driven by a Class E PA. The impedance effects are particularly investigated in order to derive conditions for a maximized efficiency of an example 6.78 MHz WPT system.

Manuscript received December 24, 2015; revised April 10, 2016; accepted May 2, 2016. This work was supported by Shanghai Natural Science Foundation under Grant 16ZR1416300.

M. Fu is with Center for Power Electronics Systems, Virginia Polytechnic Institute and State University, Blacksburg, VA 24061, USA (e-mail: minfanfu@vt.edu). H. Yin, M. Liu, and C. Ma are with University of Michigan-Shanghai Jiao Tong University Joint Institute, Shanghai Jiao Tong University, Minhang, Shanghai 200240, P. R. China (e-mail: yyy@sjtu.edu.cn; mikeliu@sjtu.edu.cn; chbma@sjtu.edu.cn). C. Ma is also with a joint faculty appointment in School of Mechanical Engineering, Shanghai Jiao Tong University.

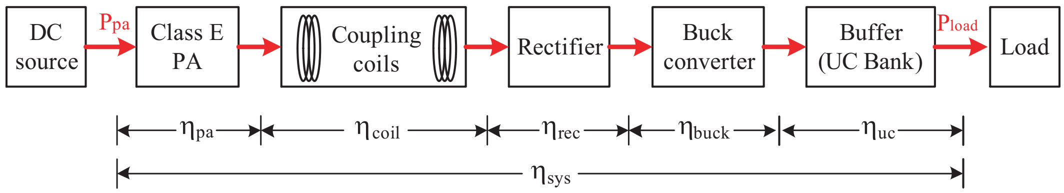

Fig. 1. System configuration.

Then the combination of loading control and energy buffering is proposed to simultaneously achieve high efficiency and meet different power demands. A buck converter and an ultracapacitor (UC) bank are added in the 6.78 MHz WPT system as two new degrees of freedom to implement the efficiency and power control, respectively. The UC bank works as an energy buffer to decouple the actual load power from the WPT system. This further simplifies the design and control of a Class E PA driven MHz WPT system that always operates under its desired condition. Instead of the conventional electrolytic capacitors such as a common tantalum capacitor, here the UC is chosen as the energy buffer due to its much higher capacitance [31]. The proposed control scheme makes it possible to efficiently charge and supply power to various electronic devices using a same transmitter, and thus potentially improves the functionality and adaptivity of the WPT systems.

It is known that the so-called varying frequency control and varying bus voltage (PA dc input voltage) control have also been proposed for the output power regulation and control [32]. However, both the control methods require a relatively complicated control algorithm. Besides, dedicated hardware is needed to measure, communicate, calculate, and implement the control; while in the proposed power control, only an energy buffer and simple on/off control of the PA are required. And more importantly, the sensitive Class E PA always efficiently works under its desired loading condition and power level. The sizing of the UCs can also be minimized for a target application. In addition, new technologies, nanotechnology and Li-ion-based hybrid UC such as the Li-ion Capacitor (LIC), can be applied to further improve the energy density of the UCs and thus significantly decrease the size of the UC bank for energy buffering purposes [33], [34].

II. Optimal Conditions for High Efficiency

The configuration of the 6.78 MHz WPT system proposed in this paper is shown in Fig. 1. It consists of a Class E PA, two coupling coils, a full-bridge rectifier, a buck converter, an UC bank, and a load. The buck converter and the UC bank are combined together to maintain a high efficiency of the Class E PA driven MHz WPT system, as discussed in the following sections. Here the overall system efficiency η_{sys} is defined as

$$\eta_{sys} = \frac{P_{load}}{P_{pa}}, \tag{1}$$

where P_{load} is the power received by the load, and P_{pa} is the input power from the dc source. η_{sys} can also be represented as

$$\eta_{sys} = \eta_{pa} \cdot \eta_{coil} \cdot \eta_{rec} \cdot \eta_{buck} \cdot \eta_{uc}, \tag{2}$$

where η_{pa}, η_{coil}, η_{rec}, η_{buck}, and η_{uc} are the efficiencies of PA, coupling coils, rectifier, buck converter, and UC bank, respectively.

Note the concept of the Class E PA driven WPT system itself is not new [28]. Meanwhile, due to the high loading sensitivity of the PA, the characteristics of the overall WPT systems may significantly change with different topologies and under various loading conditions. Thus, as discussed below, it is especially important to analyze the impedance characteristics at a system level, i.e., from the PA to the final load. This analysis serves as a basis to derive a condition that maximizes the system efficiency in a dynamic environment such as with varying coil relative position and/or load.

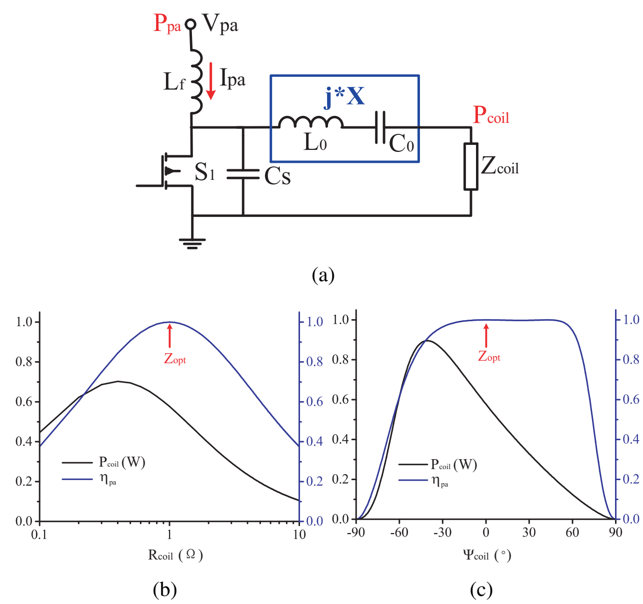

Fig. 2. A Class E power amplifier. (a) Circuit model. (b) Efficiency and output power versus R_{coil} when $X_{coil} = 0$. (c) Efficiency and output power versus Ψ_{coil} when $R_{coil} = 1\Omega$.

A. PA Load Analysis in WPT System

Here the requirement from the Class E PA is discussed when it is used as a power source in the MHz WPT system. The circuit for a classical Class E PA is shown in Fig. 2 (a), where L_f is a radio frequency (RF) choke; S_1 is a switch; C_s is a shunt capacitor. L_0 and C_0 work as an impedance matching network with a net reactance jX. V_{pa} and I_{pa} are the input voltage and current of the PA. For a target load Z_{opt}, the circuit parameters can be optimized under any operating frequency ω

using Raab's equations,

$$\begin{cases} B = \omega C_s = \frac{8}{\pi(\pi^2+4)Z_{opt}} \approx \frac{0.184}{Z_{opt}} \\ X = \omega L_0 - \frac{1}{\omega C_0} = \frac{\pi(\pi^2-4)}{16} Z_{opt} \approx 1.15 Z_{opt} \end{cases}, \tag{3}$$

where B is the susceptance of C_s [29], [30]. Under the optimized B and X, the PA output power and efficiency, P_{coil} (i.e., the input power of the coupling coils) and η_{pa}, are analytically derived as follows for any coil input impedance, Z_{coil} (=$R_{coil} + jX_{coil}$),

$$\begin{cases} P_{coil} = \frac{V_{pa}^2 g^2 R_{coil}}{2R_{pa}^2} \\ \eta_{pa} = \frac{g^2 R_{coil}}{2R_{pa}} \end{cases}, \tag{4}$$

where

$$g = \frac{\pi \sin\phi_1 + 2\cos\phi_1}{2\cos\phi \sin\phi_1 + \pi/2 \cos\psi}, \tag{5}$$

$$R_{pa} = \frac{\pi^2/4 - g[\pi/2\cos\phi + \sin\phi]}{\pi B}, \tag{6}$$

$$\psi = \tan^{-1}\left(\frac{X + X_{coil}}{R_{coil}}\right), \tag{7}$$

$$\phi = \tan^{-1}\left[\frac{(\pi^2/2-4) - \pi B R_{coil}\rho(2\cos\psi + \pi\sin\psi)}{\pi + \pi B R_{coil}\rho(\pi\cos\psi - 2sin\psi)}\right], \tag{8}$$

$$\phi_1 = \phi + \psi, \tag{9}$$

$$\rho = \sqrt{1 + \left(\frac{X + X_{coil}}{R_{coil}}\right)^2}. \tag{10}$$

All the above variables, g, R_{pa}, ψ, ϕ, ϕ_1, and ρ, relate to the coil input impedance, Z_{coil}. Using normalized parameters, V_{pa}=1 V and Z_{opt}=1 Ω, Fig. 2(b) and (c) show the influences of R_{coil} and Ψ_{coil} (phase of Z_{coil}). It is known that an optimal soft-switching condition, i.e., ZVS and ZVDS, can be achieved when $R_{coil} = Z_{opt}$ and $\Psi_{coil} = 0$ [29], [30]. Meanwhile, the two subfigures show that it is possible to efficiently operate the PA over a narrow range of the load around Z_{opt}. Beyond this range the inefficiency of the PA may cause system failure or even damage the switch S_1. In real applications variations in the final load and relative position of coils will inevitably lead to a varying Z_{coil}. It is important to actively control Z_{coil} for a robust and high-efficiency operation of the Class E PA driven WPT system.

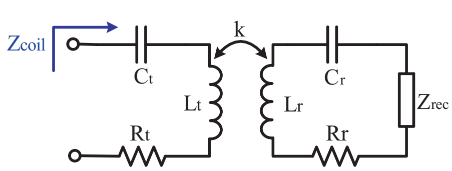

Fig. 3. Circuit model of the coupling coils.

As shown in Fig. 3, L, C, and R with different subscripts (t and r) represent the coil inductors, compensated capacitors and parasitic resistors of the transmitting and receiving coils; k is the coupling coefficient, and Z_{rec} (=$R_{rec} + jX_{rec}$) is the input impedance seeing into the following full-bridge rectifier. Under resonance,

$$j\omega L_t + \frac{1}{j\omega C_t} = 0 \text{ and } j\omega L_r + \frac{1}{j\omega C_r} = 0, \tag{11}$$

thus the load of the PA, i.e., Z_{coil}, can be derived [11],

$$\begin{cases} Z_{coil} = R_t + \frac{\omega^2 k^2 L_t L_r}{R_r + R_{rec} + jX_{rec}}, \\ R_{coil} = R_t + \frac{\omega^2 k^2 L_t L_r (R_r + R_{rec})}{(R_r + R_{rec})^2 + X_{rec}^2}, \\ X_{coil} = -\frac{\omega^2 k^2 L_t L_r X_{rec}}{(R_r + R_{rec})^2 + X_{rec}^2}. \end{cases} \tag{12}$$

The efficiency of the coupling coils can then be calculated,

$$\eta_{coil} = \frac{R_{coil} - R_t}{R_{coil}} \cdot \frac{R_{rec}}{R_{rec} + R_r}. \tag{13}$$

It can be seen that both Z_{coil} and η_{coil} relate to k (i.e., the relative position of coils) and Z_{rec}, namely the characteristics of the following circuits. Considering the complicated interactions among the circuits and unavoidable uncertainties in a real WPT system, system-level analysis is very important that guides the optimization of the overall system performance.

B. System-level Efficiency Optimization

Fig. 4 shows a simplified circuit model of the WPT system including the PA, the coupling coils, the rectifier, and a load R_{buck}. For this system, its efficiency η_{pa2rec} is

$$\eta_{pa2rec} = \frac{P_{buck}}{P_{pa}} = \eta_{pa} \cdot \eta_{coil} \cdot \eta_{rec}, \tag{14}$$

where P_{buck} is the power received by the load R_{buck}. Although both η_{pa} and η_{coil} can be analytically derived, as shown in (4) and (13), it is challenging to derive η_{rec} due to the complex nonlinear behaviors of the diodes at MHz. Instead well-known RF circuit simulation software, the Advanced Design System (ADS) from Keysight Technologies, is used to numerically calculate the efficiencies, η_{pa}, η_{coil}, η_{rec}, and thus η_{pa2rec} under various R_{buck}.

As shown in Fig. 2(b)(c), it is important to first determine a target load, i.e., Z_{opt}, for the Class E PA due to its narrow range of the load for high efficiency. It is known that at a same power level a small Z_{opt} increases the power losses caused by components' parasitic resistances, and significantly lowers the efficiencies of both PA and coupling coils. A large Z_{opt} is usually preferred in terms of efficiency. Meanwhile, a large Z_{opt} requires a large V_{pa} to provide a given P_{coil} and increases the voltage stress on S_1 ($\approx 3.6V_{pa}$) [29], [30]. In this paper the breakdown voltage of S_1 is 150 V, which means the maximum V_{pa} can not exceed 42 V (=150/3.6). Considering the possible deviation from Z_{opt} in real applications, here V_{pa} is chosen as 30 V to ensure a safe margin. In order to achieve a target power level, 20 W here, the required output power of the PA, P_{coil}, can be approximately estimated, which is about 24 W. Given the specified V_{pa} and P_{coil}, a 15 Ω Z_{opt} is then determined according to (4). All the circuit parameters of the PA and the coupling coils are labeled in Fig. 4. L_f is a RF choke with low parasitic resistance (0.12 Ω), and L_0 is a high-Q (310) inductor at 6.78 MHz. The other parameters of the PA are then determined using the Raab's equations, (3). The inductances and the parasitic resistances of the coupling coils are measured by a Vector Network Analyzer (VNA) and compensated using the two capacitors, C_t and C_r [refer to (11)]. In the simulation the SPICE models for the switch S_1 (SUD15N15) and diodes

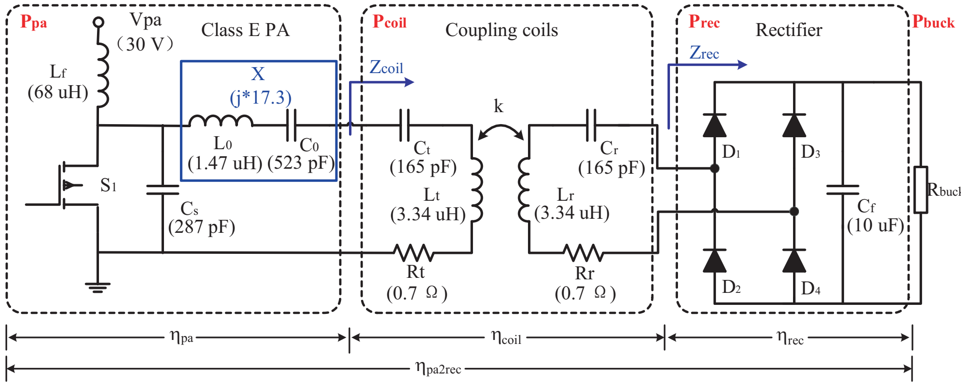

Fig. 4. Simplified circuit model of the WPT system.

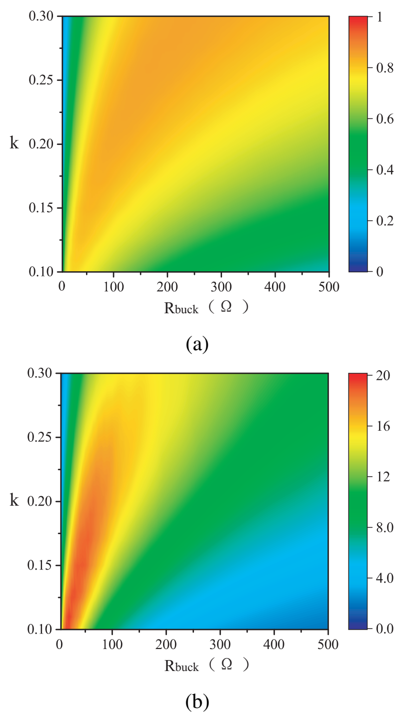

Fig. 5. η_{pa2rec} and P_{buck} versus R_{buck} and k. (a) η_{pa2rec}. (b) P_{buck} (W).

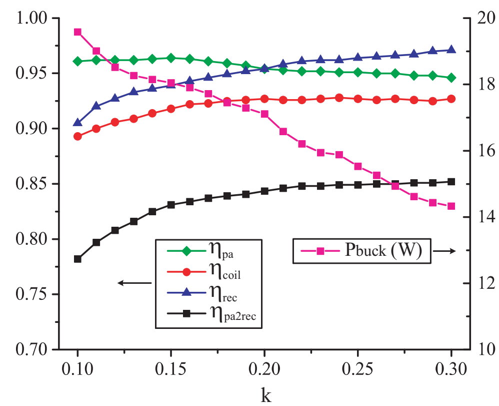

Fig. 6. Efficiencies and output power under various k and its corresponding $R_{buck,opt}$.

D_1–D_4 (STPSC406) are used to accurately predict behavior of the WPT system.

The relationships among R_{buck}, k, η_{pa2rec}, and P_{buck} are investigated and shown in Fig. 5(a)(b). Note here P_{buck} is the output power of the rectifier. It is desirable to observe that the range of high system efficiency largely overlaps with that of high output power. The efficiencies and the output power under various k and its corresponding $R_{buck,opt}$, a R_{buck} maximizing η_{pa2rec}, are shown in Fig 6. By having the optimal $R_{buck,opt}$'s, not only η_{pa2rec} (black curve) but also η_{pa} (green curve) can be maintained at a high level over a wide range of k. This result indicates that by tracking the optimal $R_{buck,opt}$'s, the robustness of the system performance such as the system efficiency can be improved when there are variations in k (i.e., relative position of coils) and/or the characteristic of the final load.

Besides, it should be noted that the output power P_{buck} in Fig. 6 actually decreases with a larger k. This is because of the capacitive Z_{rec} caused by the diodes' strong nonlinearity at MHz. The nonlinearity further leads to an inductive Z_{coil} under the optimal $R_{buck,opt}$'s, as shown in Fig. 7(a). From Fig. 7(b) it can be seen that an increasing imaginary part (i.e., phase) of the load Z_{coil} has limited effects on PA efficiency, but lowers the PA output capability and thus P_{buck}.

The above results show that the optimal $R_{buck,opt}$'s can guarantee a high-efficiency power transfer from the Class E PA to the rectifier. Thus here this operating condition is defined as a nominal condition for the MHz WPT system. It should be noted that since the determination of the optimal $R_{buck,opt}$'s is through a system-level approach, the above nominal condition does not necessarily guarantee that all the individual circuits will also operate optimally. For instance, the capacitive Z_{rec} means the receiving coil does not completely resonate, and it lowers the coupling coil efficiency, η_{coil} [refer to (12) and (13)]; the inductive Z_{coil} also indicates the Class E PA may not work exactly at its optimal condition (i.e., ZVS and ZVDS), but the PA still operates within the range for high efficiency [refer to Fig. 7(b)]. Therefore, the above so-called nominal operating condition is a compromised solution emphasizing the performance of the overall MHz WPT system.

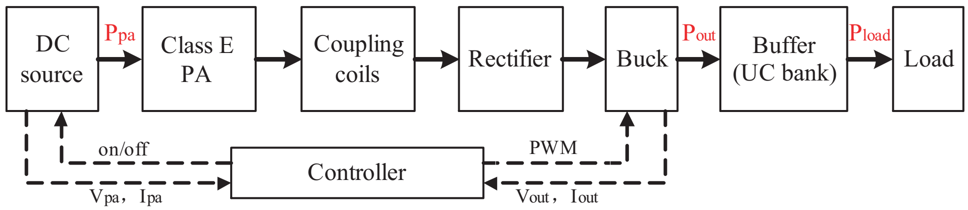

Fig. 9. Blockdiagram of control system.

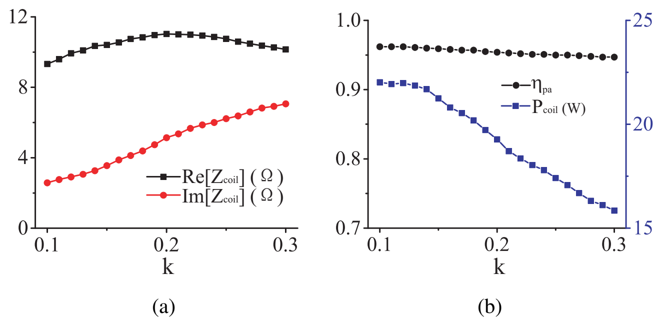

Fig. 7. The performance of PA under various $R_{buck,opt}$'s. (a) Load Z_{coil}. (b) PA efficiency and output power. Note: $Re\{*\}$ and $Im\{*\}$ mean the real and imaginary parts of a complex number, respectively.

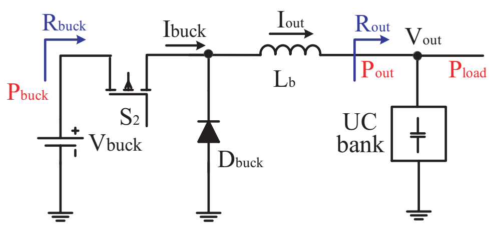

Fig. 8. The circuit of buck converter and UC bank.

III. Control of Efficiency and Power

A. Loading Control using Buck Converter

The loading control has been widely used in kHz WPT systems, such as through dc-dc converters, mostly for power control purposes [4]. The dc-dc converter was recently applied in a 13.56 MHz WPT system for a maximum efficiency tracking [24]. However, the PA (a standard RF one) efficiency is not included in the calculation of the system efficiency. A bulky bi-directional coupler is also needed to measure the input power. In this paper, the maximum dc-to-dc efficiency including the PA efficiency is tracked using a dc-dc converter, a buck converter here. More importantly, the load sensitive Class E PA further requires a system-level analysis and optimization that derives the condition for an effective loading control, as discussed in the previous section. Here a buck converter can be used to implement the control of R_{buck} in Fig. 8, the load seen by the full-bridge rectifier. V_{buck}, V_{out}, I_{buck}, and I_{out} are the input and output voltages and currents of the buck converter, respectively. For an ideal buck converter working in continuous mode, namely a large L_b,

$$D = \frac{V_{out}}{V_{buck}} = \frac{V_{out}}{\sqrt{R_{buck}P_{buck}}}, \tag{15}$$

where D is the duty cycle of the switch S_2. Since P_{buck} relates to R_{buck}, an optimal D exists for each $R_{buck,opt}$ that corresponds to a specific relative position of coils, i.e., k [refer to Fig. 5(a)(b)]. Thus maximized system efficiency can be maintained by tracking the changing $R_{buck,opt}$ through the duty cycle control of the buck converter.

Note in a buck converter V_{buck} should be greater than V_{out}. Thus a constraint is that

$$R_{out} = \frac{V_{out}^2}{P_{out}} < R_{buck,opt}, \tag{16}$$

where R_{out} is the load of the buck converter and P_{out} is its output power [see Fig. 8]. It is important to carefully choose the circuit parameters of the converter in oder to guarantee a sufficient tracking capability. Otherwise, other dc-dc converters could be considered such as boost converter and buck-boost converter.

B. Power Control using Ultracapacitors

In real applications the required power levels and types may vary significantly for different loads. In order to maintain a high system efficiency, a UC bank is added between the buck converter and the load [see Figs. 8 and 9]. It works as an energy buffer to deliver power and temporarily store energy. Thus the power requirement of a load is decoupled from the actual output power of the WPT system. This advantage is particularly useful for the Class E PA driven MHz WPT system due to the PA's high sensitivity to the operating condition. There certainly exists a trade-off between improved performance and added complexity, size, and cost, etc. Meanwhile, small UC units are already being used in today's electronic devices as energy buffers that protect microcomputers from power shutdowns, maintain the contents of CMOS memories, and assist batteries when starting computation-heavy applications, etc [35]. The new technologies such as the nanotechnology and Li-ion-based hybrid UC could further miniaturize the size of the required UC bank. The discussion here actually extends the application of UCs into a new field, the power control in MHz WPT systems.

In order to avoid overcharge, the UC bank need operate under a maximum permissible voltage, $V_{out,max}$; while its minimum voltage ($V_{out,min}$), i.e., its energy storage capability, should be determined based on the requirements from the loading condition of the buck converter and a target application. The on/off control of PA can be performed to guarantee the desired range of UC voltage variation, as summarized in the following subsection. Note that the existing devices usually operate at a fixed input dc voltage. This requirement was originally developed for the conventional physically connected systems. For the proposed WPT system, a dc-dc converter can be added to provide a fixed output voltage, which is a common practice. Meanwhile, WPT provides new possibility to directly transfer a required amount of power in a non-contacting manner. In this paper, the output power is controlled by combining the UC bank and the on/off control of the Class E PA. It may indicate a new possible configuration of the WPT systems, through which the WPT system directly outputs the required power with a high efficiency.

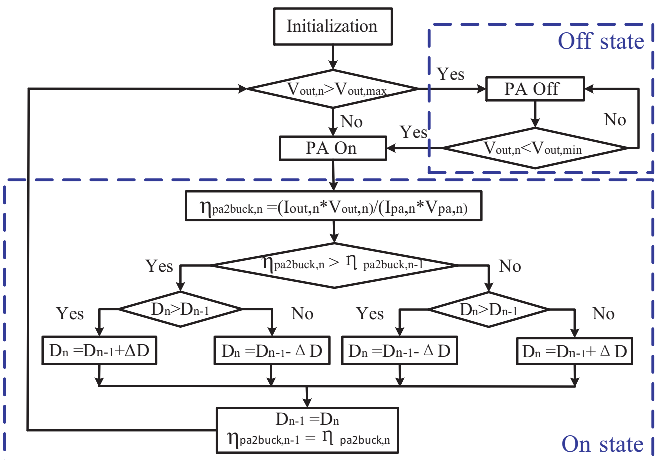

Fig. 10. Control flowchart.

C. PA On/off Control with Maximum Efficiency Tracking

The blockdiagram of the control system is shown in Fig. 9. In the on/off control of PA, the two states, "on" and "off" states, are automatically switched according to the UC voltage, i.e., V_{out} in Fig. 8:

1) "On" state: The PA is turned on when V_{out} reaches $V_{out,min}$, and the buck converter works to track $R_{buck,opt}$ for a maximized $\eta_{pa2buck}$, i.e., $\eta_{pa2rec}\times\eta_{buck}$. Usually a high η_{buck}, greater than 90%, can be maintained over a wide range of its load [24]. Thus η_{buck} has a limited influence on the value of $R_{buck,opt}$. In the "on" state P_{load} is supplied by the WPT system, and the UC bank is charged using the rest of P_{out}, i.e., $P_{out}-P_{load}$.
2) "Off" state: The PA is turned off when V_{out} reaches $V_{out,max}$. P_{load} is then completely provided by discharging the UC bank.

As shown in Fig. 9, in the "on" state a feedback mechanism is implemented to track the maximum system efficiency $\eta_{pa2buck}$, i.e., $(V_{out}I_{out})/(V_{pa}I_{pa})$.

The flow of the control is summarized in Fig. 10, where n is the newest sampling instant. $V_{pa,n}$, $I_{pa,n}$, $V_{out,n}$, and $I_{out,n}$ are the sampled input/output voltages and currents, respectively. Thus the system efficiency $\eta_{pa2buck,n}$ can be obtained in real time by calculating $(V_{out,n}I_{out,n})/\ (V_{pa,n}I_{pa,n})$. D is the duty cycle of the buck converter that controls the equivalent load resistance seen by the rectifier, i.e., R_{buck}. The system is initialized with D=0, and the state, "on" or "off", of the PA is determined according to the present UC voltage $V_{out,n}$. In the "on" state, a small and constant perturbation, ΔD, is applied in a step-by-step manner in order to change R_{buck}, and the system efficiency variation $\Delta\eta_{pa2buck}$(=$\eta_{pa2buck,n}$-$\eta_{pa2buck,n-1}$) is measured. If $\Delta\eta_{pa2buck}$ is positive, the adjusted R_{buck} approaches its optimal value. Thus a perturbation with a same sign needs to be applied in the following stage, and vice versa. This perturbation and observation (P&O) based tracking is iteratively repeated until the maximum $\eta_{pa2buck}$ is reached.

IV. Experimental verification

The final experimental MHz WPT system is shown in Fig. 11. The system consists of a programmable dc source, a 6.78 MHz Class E PA, two coupling coils, a full-bridge rectifier, a buck converter, a UC bank, a digital controller (National Instrument myRIO), and an electronic load. NI myRIO controls the on/off of the dc source via USB, and records V_{pa} and I_{pa}, i.e., the input power of the WPT system. The output voltage and current of the buck converter, V_{out} and I_{out}, are sampled through an I/V sampling board and sent to NI myRIO as well. Thus $\eta_{pa2buck}$ can be calculated and tracked in real time through the P&O-based tracking using the buck converter ($\Delta D = 0.02$). The programmable electronic load is also controlled by NI myRIO to emulate various power levels and types of the load, P_{load}. The circuit parameters are given in section II-B [refer to Fig. 4 and the types of diodes and switch]. Two coils are aligned along their vertical axes with distance d, as shown in Fig. 11(c). Table I lists the parameters and specifications of the buck converter and the UC bank. Note that the experimental setup in Fig. 11 is for validation purposes. In real applications, the NI myRIO embedded controller and the sampling board could be replaced by dedicated chips. Again, the size of the UC bank can be minimized targeting a specific application. New technologies, the nanotechnology and Li-ion-base hybrid UC, also help to significantly improve the energy density of the UCs, i.e., a much smaller size of the UC bank.

TABLE I
Parameters of Buck Converter and UC Bank.

Buck converter	Switch S_2	IFR540N (IR)
	Diode D_{buck}	BYV29 (NXP)
	Inductor L_b	100 μH
	Switching frequency	40 kHz
UC bank	Cell	BCAP0100 (Maxwell)
	Capacitance	100 F (cell)
	Internal resistance	90 mΩ (cell)
	Connection	6 cells in series (bank)
	$V_{out,min}$, $V_{out,max}$	10 V, 15 V (bank)

A. Static Characteristics

First the electronic load is directly connected with the rectifier. The buck converter and the UC bank are not included. The static characteristics of the WPT system are measured in order to validate the previous theoretical analysis in section II-B. During the measurement, the vertical coil distance d changes from 15 mm to 45 mm that corresponds to a varying coupling

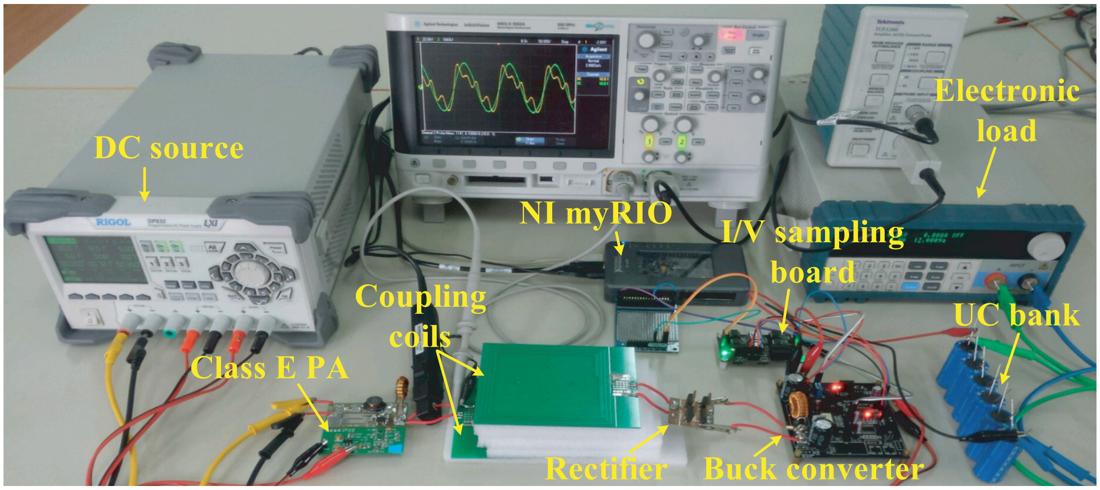

(a)

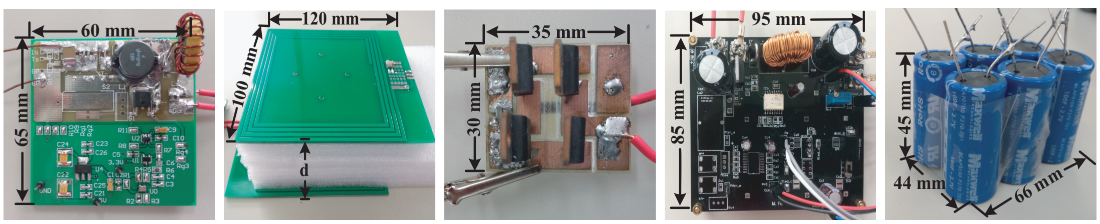

(b) (c) (d) (e) (f)

Fig. 11. Experimental setup. (a) Overall system. (b) 6.78 MHz Class E PA. (c) Coupling coils. (d) Full-bridge rectifier. (e) Buck converter. (f) UC bank.

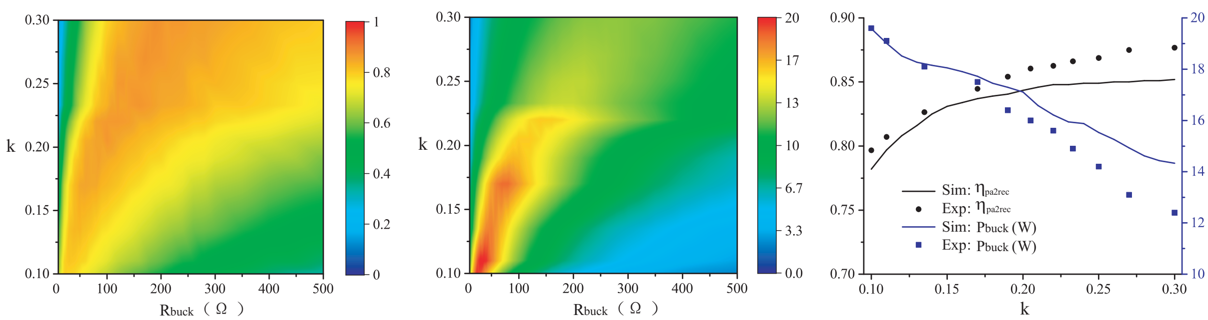

(a) (b) (c)

Fig. 12. Measured static characteristics. (a) η_{pa2rec} versus R_{buck} and k. (b) P_{buck} (W) versus R_{buck} and k. (c) Optimal η_{pa2rec} and P_{buck} versus k.

coefficient k from 0.31 to 0.09. At each d, η_{pa2rec} and P_{buck} are measured under different R_{buck}, as shown in Fig. 12(a)(b). The experimental results are consistent with the simulation ones in Fig. 5. Measured variations in the optimal η_{pa2rec} and P_{buck} under various k and its corresponding $R_{buck,opt}$ in Fig. 12(c) also well match the previous simulation results.

B. Dynamic Tracking and Power Control

Then all the function blocks in Fig. 9 are included in the experiments. In the scenario five cases are designed with different coil distances d (i.e., k) and various levels and types of the load power P_{load} [see Fig. 13 (a)]. The dynamic responses of power (P_{pa}, P_{out}, and P_{load}) and the output voltage/current (V_{out} and I_{out}) of the buck converter are shown in the two following subfigures, Fig. 13 (b)(c). In periods T_1–T_3, d is fixed at 4 cm and constant load power profiles are applied with levels of 10, 5, and 1 W, respectively. Under the tracking control using the buck converter the maximum efficiency of $\eta_{pa2buck}$ is quickly reached with a response time of less than 0.5 s. In all the three "on" states the Class E PA works at a stable input power level of 24 W despite different levels of the actual load power; while in the "off" states UC bank is discharged to continuously supply the require constant load power. Under the on/off control the UC bank is properly charged and discharged within the prescribed voltage range, i.e., V_{out} between $V_{out,min}$ and $V_{out,max}$. A high $\eta_{pa2buck}$, the ratio of P_{out} to P_{pa} in Fig. 13(b), is maintained in the "on" states, and their average values $\eta_{pa2buck,avg}$ are listed in Fig. 13(a). The average overall system efficiency from the dc source to the load, $\eta_{sys,avg}$ is also shown in the subfigure. The discussion on the efficiencies is summarized later at the end of this subsection. Note P_{out} slightly increases in

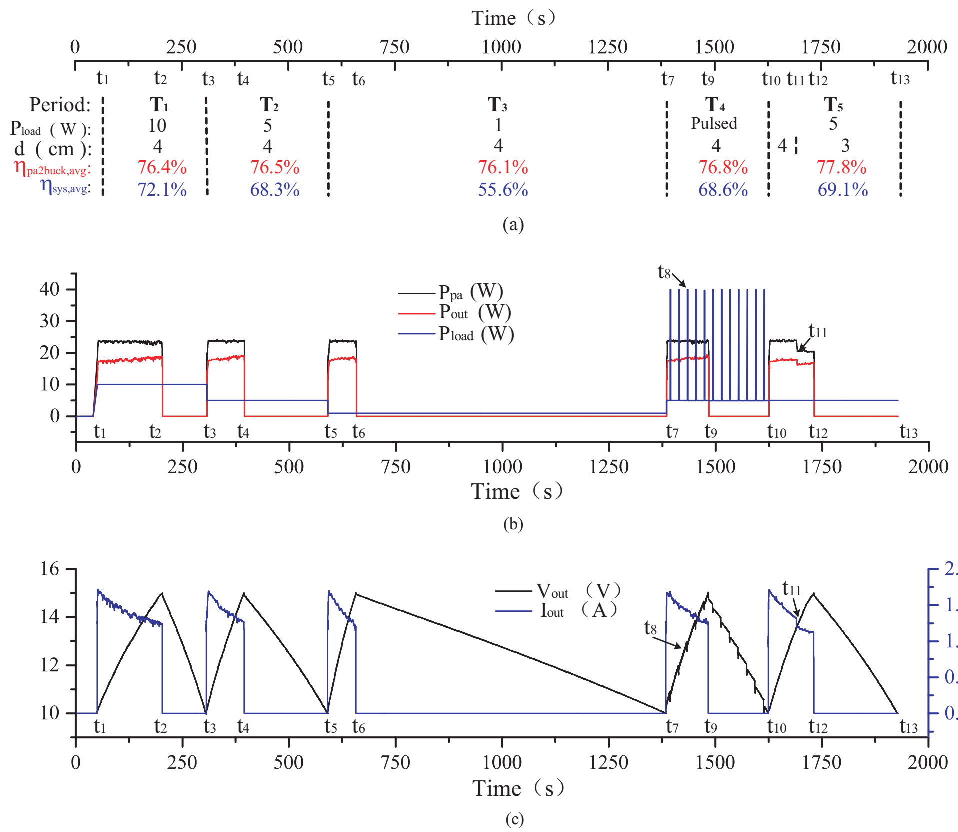

Fig. 13. Experimental results under different coil distances and various constant and pulsed load power profiles.

the “on” states because higher the UC voltage higher the efficiency of the buck converter. As an example, the drain-source voltage of S_1, i.e., the switch in the Class E PA, is given in Fig. 14 during period T_1. The waveform is close to but not as same as the optimal waveform of a Class E PA under ZVS and ZVDS operation. This result verifies that the proposed solution is a compromised one that maximizes the overall system performance rather than the performances of individual circuits [refer to section II-B].

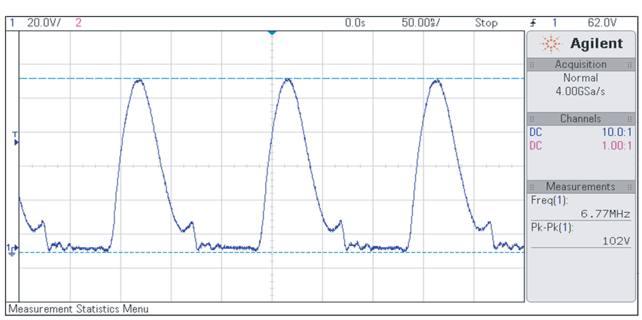

Fig. 14. Drain-source voltage of switch S_1 in the Class E PA.

In period T_4 a pulsed load profile with two power levels of 5 and 40 W is applied and d is still 4 cm. The peak power, 40 W, lasts for 1 s and appears every 20 s. It is interesting to note that the peak power is actually higher than P_{pa}(=24 W), the input power of the WPT system. Using the UC bank as an energy buffer P_{pa} and P_{out} are almost not affected by the final pulsed load power. Small fluctuations in V_{out} can be observed such as at t_8 in Fig. 13(c). This explains the function of the UC bank to temporarily store/deliver energy and thus decouple the output power of the WPT system and the required load power. The experimental results also show that the proposed WPT system responses fast under this extreme loading condition. Thanks to the UC bank, the actual load is decoupled with the WPT system. Thus the response speed is only determined by the power delivery capability of the UC bank, an energy storage device well-known for its very high power density [36].

In period T_5 the power profile is again a constant one, but d changes from 4 cm to 3 cm at t_{11}. From the previous analysis in section II-B the optimal $R_{buck,opt}$ will change too. As shown in Fig. 13(b), the new $R_{buck,opt}$ is quickly tracked within 0.1 s at t_{11}. The speed of tracking is faster than that at t_1, 0.5 s, because the starting point of the tracking at t_{11} is closer to the optimal point. P_{pa} and thus P_{out} drop at t_{11} due to the smaller d, namely a larger k [refer to Fig. 12(c)].

Finally, as shown in Fig. 13(a), high efficiency from the dc source to the buck converter, $\eta_{pa2buck}$ is achieved in all the five cases. Meanwhile, the efficiency from the dc source to the load, η_{sys} in (2), becomes lower when the load power is small such as 1 W in T_3. It is because smaller load power requires the UC bank to temporarily store larger energy, and thus more loss occurs due to the UC internal resistance. For a specific application an optimized sizing of the UC bank could be discussed to minimize its energy loss. It is interesting to note that at a similar average power level, 5 W in T_2 and 6.75

W in T_4, almost same efficiencies are achieved despite the quite different load profile in T_4, a pulsed one.

V. Conclusion

This paper first provides a system-level analysis on a 6.78 MHz WPT system driven by a Class E PA. A control scheme is then developed that maintains high system efficiency under uncertainties and various power demands. A buck converter and a UC bank are introduced as two new degrees of freedom to implement the efficiency and power control, respectively. Experimental results show that the proposed control scheme can quickly track the maximum system efficiency and supply the required power, both constant and pulsed ones, at various power levels. Thus the scheme enables the Class E PA driven WPT system to always work under its desired operating condition despite different power requirement, load characteristic, and transfer distance. This advantage simplifies the design, and improves the functionality and adaptivity of a WPT system. The proposed control scheme is particularly suitable for the MHz WPT systems driven by the load sensitive Class E PA. Meanwhile, the concept itself is a general one that can be applied in the MHz WPT systems with other topologies.

References

[1] A. P. Sample, B. H. Waters, S. T. Wisdom, and J. R. Smith, "Enabling seamless wireless power delivery in dynamic environments," *Proc. IEEE*, vol. 101, no. 6, pp. 1343–1358, Apr. 2013.

[2] S. Y. R. Hui, W. Zhong, and C. K. Lee, "A critical review of recent progress in mid-range wireless power transfer," *IEEE Trans. Power Electron.*, vol. 29, no. 9, pp. 4500–4511, 2014.

[3] J.-U. W. Hsu, A. P. Hu, and A. Swain, "A wireless power pickup based on directional tuning control of magnetic amplifier," *IEEE Trans. Ind. Electron.*, vol. 56, no. 7, pp. 2771–2781, 2009.

[4] N. Keeling, G. Covic, J. T. Boys *et al.*, "A unity-power-factor IPT pickup for high-power applications," *IEEE Trans. Ind. Electron.*, vol. 57, no. 2, pp. 744–751, 2010.

[5] F. van der Pijl, P. Bauer, and M. Castilla, "Control method for wireless inductive energy transfer systems with relatively large air gap," *IEEE Trans. Ind. Electron.*, vol. 60, no. 1, pp. 382–390, 2013.

[6] U. K. Madawala, M. Neath, and D. J. Thrimawithana, "A power–frequency controller for bidirectional inductive power transfer systems," *IEEE Trans. Ind. Electron.*, vol. 60, no. 1, pp. 310–317, 2013.

[7] H. Li, K. W. Jie Li, W. Chen, and X. Yang, "A maximum efficiency point tracking control scheme for wireless power transfer systems using magnetic resonant coupling," *IEEE Trans. Power Electron.*, vol. 30, no. 7, pp. 3998–4008, 2015.

[8] W. Zhong and S. Hui, "Maximum energy efficiency tracking for wireless power transfer systems," *IEEE Trans. on Power Electron.*, vol. 30, no. 7, pp. 4025–4034, July 2015.

[9] J. J. Casanova, Z. N. Low, and J. Lin, "Design and optimization of a class-E amplifier for a loosely coupled planar wireless power system," *IEEE Trans. Circuits Syst. II, Exp. Briefs*, vol. 56, no. 11, pp. 830–834, 2009.

[10] D. Ahn and S. Hong, "Effect of coupling between multiple transmitters or multiple receivers on wireless power transfer," *IEEE Trans. Ind. Electron.*, vol. 60, no. 7, pp. 2602–2613, 2013.

[11] M. Fu, T. Zhang, C. Ma, and X. Zhu, "Efficiency and optimal loads analysis for multiple-receiver wireless power transfer systems," *IEEE Trans. Microw. Theory Tech.*, vol. 63, no. 3, pp. 801–812, 2015.

[12] W. Chen, R. Chinga, S. Yoshida, J. Lin, C. Chen, and W. Lo, "A 25.6 W 13.56 MHz wireless power transfer system with a 94% efficiency gan class-e power amplifier," in *2012 IEEE MTT-S International Microwave Symposium Digest*, Montreal, Canada, Jun. 2012.

[13] J.-H. Choi, S.-K. Yeo, S. Park, J.-S. Lee, and G.-H. Cho, "Resonant regulating rectifiers (3R) operating for 6.78 MHz resonant wireless power transfer (RWPT)," *IEEE J. Solid-State Circuits*, vol. 48, no. 12, pp. 2989–3001, 2013.

[14] A. Rajagopalan, A. K. RamRakhyani, D. Schurig, and G. Lazzi, "Improving power transfer efficiency of a short-range telemetry system using compact metamaterials," *IEEE Trans. Microw. Theory Techn.*, vol. 62, no. 4, pp. 947–955, 2014.

[15] D. Ahn and S. Hong, "Wireless power transmission with self-regulated output voltage for biomedical implant," *IEEE Trans. Ind. Electron.*, vol. 61, no. 5, pp. 2225–2235, 2014.

[16] N. Kim, K. Kim, J. Choi, and C.-W. Kim, "Adaptive frequency with power-level tracking system for efficient magnetic resonance wireless power transfer," *Electronics letters*, vol. 48, no. 8, pp. 452–454, 2012.

[17] "Improving the effectiveness, flexibility and availability of spectrum for short range devices," in *Document RAG07-1/17-E, , Radiocommunication Advisory Group, International Telecommunication Union*, 2007.

[18] J. Park, Y. Tak, Y. Kim, Y. Kim, and S. Nam, "Investigation of adaptive matching methods for near-field wireless power transfer," *IEEE Trans. Antennas Propag.*, vol. 59, no. 5, pp. 1769–1773, 2011.

[19] T. C. Beh, M. Kato, T. Imura, S. Oh, and Y. Hori, "Automated impedance matching system for robust wireless power transfer via magnetic resonance coupling," *IEEE Trans. Ind. Electron.*, vol. 60, no. 9, pp. 3689–3698, 2013.

[20] K. K. Ean, B. T. Chuan, T. Imura, and Y. Hori, "Impedance matching and power division using impedance inverter for wireless power transfer," *IEEE Trans. Ind. Appl.*, vol. 50, no. 3, pp. 2061–2070, 2014.

[21] S. Aldhaher, P. C. Luk, and J. F. Whidborne, "Tuning class E inverters applied in inductive links using saturable reactors," *IEEE Trans. Power Electron.*, vol. 29, no. 6, pp. 2969–2978, 2014.

[22] S. Aldhaher, P. Luk, and J. Whidborne, "Electronic tuning of misaligned coils in wireless power transfer systems," *IEEE Trans. Power Electron.*, vol. 29, no. 11, pp. 5975 – 5982, 2014.

[23] M. Fu, C. Ma, and X. Zhu, "A cascaded boost-buck converter for high efficiency wireless power transfer systems," *IEEE Trans. Ind. Informat.*, vol. 10, no. 3, pp. 1972–1980, 2014.

[24] M. Fu, H. Yin, X. Zhu, and C. Ma, "Analysis and tracking of optimal load in wireless power transfer systems," *IEEE Trans. Power Electron.*, vol. 30, no. 7, pp. 3952–3963, 2015.

[25] B. H. Waters, B. J. Mahoney, V. Ranganathan, and J. R. Smith, "Power delivery and leakage field control using an adaptive phased-array wireless power system," *IEEE Trans. Power Electron.*, vol. 30, no. 7, pp. 4025–4034, 2015.

[26] Z. N. Low, R. A. Chinga, R. Tseng, and J. Lin, "Design and test of a high-power high-efficiency loosely coupled planar wireless power transfer system," *IEEE Trans. Ind. Electron.*, vol. 56, no. 5, pp. 1801–1812, 2009.

[27] Z. N. Low, J. Casanova, P. Maier, J. Taylor, R. Chinga, and J. Lin, "Method of load/fault detection for loosely coupled planar wireless power transfer system with power delivery tracking," *IEEE Trans. Ind. Electron.*, vol. 56, no. 4, pp. 1478–1486, 2010.

[28] D. Kurschner and C. Rathge, "Maximizing dc-to-load efficiency for inductive power transfer," *IEEE Trans. Power Electron.*, vol. 28, no. 5, pp. 2437–2447, 2013.

[29] F. H. Raab, "Idealized operation of the class E tuned power amplifier," *IEEE Trans. Trans. Circuits Syst.*, vol. 24, no. 12, pp. 725–735, 1977.

[30] ——, "Effects of circuit variations on the class E tuned power amplifier," *IEEE J. Solid-State Circuits*, vol. 13, no. 2, pp. 239–247, 1978.

[31] P. Sharma and T. Bhatti, "A review on electrochemical double-layer capacitors," *Energy Conversion and Management*, vol. 51, no. 12, pp. 2901–2912, 2010.

[32] M. de Rooij and J. Strydom. (2013) Low Power Wireless Energy Converters. epc-wp-wp014.pdf. [Online]. Available: http://www.digikey.com/Web Export/Supplier Content/EfficientPowerConversion_917/PDF/epc-wp-wp014.pdf.

[33] W. Wang, S. Guo, I. Lee, K. Ahmed, J. Zhong, Z. Favors, F. Zaera, M. Ozkan, and C. S. Ozkan, "Hydrous ruthenium oxide nanoparticles anchored to graphene and carbon nanotube hybrid foam for supercapacitors," *Scientific reports*, vol. 4, 2014.

[34] K. Naoi, "Hybrid li-ion based supercapacitor systems in organic media," in *Encyclopedia of Applied Electrochemistry*. Springer, 2014, pp. 1013–1025.

[35] KEMET. Small Cell Supercapacitors. [Online] Available: http://www.kemet.com/Small Cell Supercapacitors.

[36] A. Burke and M. Miller, "The power capability of ultracapacitors and lithium batteries for electric and hybrid vehicle applications," *Journal of Power Sources*, vol. 196, no. 1, pp. 514–522, 2011.

Minfan Fu (S'13-M'16) received the B.S., M.S., and Ph.D. degrees in electrical and computer engineering from University of Michigan-Shanghai Jiao Tong University Joint Institute, Shanghai Jiao Tong University, Shanghai, China in 2010, 2013, and 2016 respectively. He is currently a visiting scholar in the Center for Power Electronics Systems (CPES), Virginia Polytechnic Institute and State University, Blacksburg, VA, USA.

His research interests include megahertz wireless power transfer, resonant converters, and circuit design optimization.

He Yin (S'13) received the B.S. degree in electrical and computer engineering from University of Michigan-Shanghai Jiao Tong University Joint Institute, Shanghai Jiao Tong University, Shanghai, China in 2012. He is currently working toward Ph.D. degree in the same institute.

His research interests include optimization and decentralized control of hybrid energy storage systems and wireless power transfer systems.

Ming Liu (S'15) received the B.S. degree from SiChuan University, Sichuan, China, in 2007, and the M.S. degree from University of Science and Technology Beijing, Beijing, China, in 2011, both in mechatronic engineering. He is currently working toward the Ph.D. degree in electrical and computer engineering, University of Michigan-Shanghai Jiao Tong University Joint Institute, Shanghai Jiao Tong University, Shanghai, China.

His research interests include component- and system-level design of megahertz wireless power transfer systems and general power electronics systems.

Chengbin Ma (M'05) received the B.S. (Hons.) degree in industrial automation from East China University of Science and Technology, Shanghai, China, in 1997, and the M.S. and Ph.D. degrees both in electrical engineering from University of Tokyo, Japan, in 2001 and 2004, respectively.

He is currently an assistant professor of electrical and computer engineering with the University of Michigan-Shanghai Jiao Tong University Joint Institute, Shanghai Jiao Tong University, China. He is also with a joint faculty appointment in School of Mechanical Engineering, Shanghai Jiao Tong University. Between 2006 and 2008, he held a post-doctoral position with the Department of Mechanical and Aeronautical Engineering, University of California Davis, USA. From 2004 to 2006, he was a R&D researcher with Servo Laboratory, Fanuc Limited, Japan.

His research interests include wireless power transfer, networked hybrid energy systems, and mechatronic control.